© Universiti Tun Hussein Onn Malaysia Publisher's Office

IJIE

http://penerbit.uthm.edu.my/ojs/index.php/ijie
ISSN : 2229-838X e-ISSN : 2600-7916

The International Journal of Integrated Engineering

Integrated Heat Regenerator (IHR) Designs with Hydrogen Preheater and Thermoelectric Generator for Power Enhancement of a 2 kW Fuel Cell Vehicle

WANW Mohamed[1], MH Hamdan[1*], NF Zamri[1], IA Zakaria[1], MF Mohamad[1], MI Rosli[2]

[1]School of Mechanical Engineering, College of Engineering,
Universiti Teknologi MARA, Shah Alam, 40450, Selangor, MALAYSIA

[2]Institut Sel Fuel,
Universiti Kebangsaan Malaysia, 43600 Bandar Baru Bangi, Selangor, MALAYSIA

*Corresponding Author

DOI: https://doi.org/10.30880/ijie.2022.14.02.021
Received 29 November 2021; Accepted 7 April 2022; Available online 02 June 2022

Abstract: The power train efficiency of fuel cell vehicles (FCV) can be enhanced by improving the hydrogen energy utilization. Based on a mini FCV running on a 2 kW open-cathode Polymer Electrolyte Membrane (PEM) fuel cell, a waste heat recovery system design needs to be developed as an approach towards higher energy efficiency. The novelty of the system is on the integration of thermoelectric generator technology with hydrogen preheating process for a combined heat and power output. This manuscript presents the proposed integrated heat regenerator (IHR) designs, analysed using numerical computational modelling. Three IHR designs were proposed where the main design criteria are (i) a minimum of 10°C hydrogen preheating degree, and (ii) non-parasitic active cooling for the Thermoelectric generator (TEG) cells. Three design concepts were studied to identify its design and performance limitations. The numerical results were validated with theoretical modelling analysis for hydrogen exit temperatures and TEG surface temperatures. The analysis on predicted fuel cell power enhancement, TEG power generation and waste heat utilization were performed by relating the temperature profiles of the hydrogen reactant and TEG surfaces to fuel cell reaction models and TEG power relationships. A compact IHR design that produced 7.7 to 8 % total power enhancement and suitable in size for a mini FCV was identified for future development works

Keywords: PEM fuel cells, hydrogen, waste heat recovery, thermoelectric generator, energy efficiency

1. Introduction

Sustainable transportation is a major driving force towards hydrogen economy. Hydrogen-powered fuel cell vehicles (FCV) are gaining attention due to its positive impact on the environment added with its capability for fast refuelling and longer driving range [1]. Rapid advances in FCV technology have produced models such as the Toyota Mirai and Honda Clarity with a driving range between 500 km to 600 km running on PEM fuel cells with higher than 60% peak efficiency [2]. Technologies contributing to hydrogen power train efficiency enhancement is important to enable FCV to be cost-competitive and sustainable. Advancements in membrane, catalyst and stack architecture has contributed in the development of fuel cell stacks with high power densities suitable for vehicle propulsion [3]. A less explored area that may contribute to the hydrogen power train efficiency is energy recovery.

Waste heat recovery (WHR) is an extended component in the thermal management system for fuel cells and can be an essential auxiliary system in future fuel cell system designs [4]. The operating temperature for open cathode, low temperature PEM fuel cell stacks is usually from 50 to 80°C [5]. The generated heat needs to be removed to avoid

*Corresponding author: hadramihamdan@gmail.com

overheating of the membrane that leads to power deterioration. Heat generation in fuel cells is a result of the exothermic electrochemical reactions between hydrogen and oxygen, as well as from the irreversibilities of the reaction. Fuel cells operating within the ohmic region generates heat at 40 to 50% from its hydrogen energy input [6] where the stack and exhaust stream temperatures are dynamically related to the adopted cooling scheme [7]. Recovery of the generated waste heat is an emerging area due to the need to enhance the techno-economics of fuel cell systems and making it attractive as compared to current energy systems. Integration of fuel cell systems with mechanical energy recovery systems have been explored. Hybrid systems such as the integration of fuel cells with Organic Rankine Cycles (ORC) was reported by He et al. [8] using R123, R245fa, R134a, water, and ethanol as the working fluid. The thermal efficiency was improved by integrating the ORC with a heat pump. Hwang et al. [9] developed a fuel cell cogeneration system that produced electrical power and hot water with 50% energy recovery capability. Khanmohammadi et al. [10] developed an integrated compressed air energy storage, PEM fuel cell and TEG system resulting in an efficiency increase to 31.85%.

For FCV, space and weight constraints eliminate the suitability of bulky mechanical energy recovery systems. Solid-state energy recovery devices with lightweight and no maintenance characteristics are highly desired for WHR in vehicles. A TEG is an emerging technology for direct conversion of thermal power into electrical power for stationary as well as mobile thermal system platforms. The Seebeck effect across the semiconductor material generates electrical energy when there is heat flow to excite the electrons within the thermo-elements of the material. A large temperature difference across the junctions of the TEG cells would translate into high heat transfer rates and electrical power generation. It is crucial for designs of TEG modules to create an effective heating and cooling conditions on both sides of the TEG cell such as proposed in the designs of Hamdan et al. [11] and Mohamed et al. [12]. Both TEG module designs apply non-parasitic active cooling to induce a greater heat transfer across the TEG cell. New TEG semiconductor materials and configurations are emerging and the conversion efficiency of TEG cells have been improved from the current 5% to at least 10% [13, 14]. This means that application of TEG technology would have a substantial positive impact on the techno-economy of thermal systems in the near future.

The power produced by a TEG module has been proven to be highly influenced by the temperature and flow rate of the waste heat stream [15]. However, WHR using TEG from thermal systems is viable even for low temperature streams and it can be effectively performed through concurrent thermal engineering efforts for optimal heating and cooling of the TEG cells. Compact plate-fin heat exchanger has been shown to significantly improve the heat transfer across the TEG cells [16]. Sulaiman et al. [17, 18] integrated a TEG cell, a heat pipe and a heat sink for low-grade heat recovery from a PEM fuel cell where 200 to 250 µW of electrical power was produced from a low temperature PEM fuel cell waste stream. Guo et al. [19] developed a module using a regenerator and TEG cells for WHR from a high temperature PEM fuel cell. The energy efficiency was reportedly increased between 12.4 to 19.1%. A module for heat recovery from a 2 kW PEM fuel cell applied a 4-cell TEG configuration with a double heat sink to assist active cooling that is dynamically related to the motion of the fuel cell vehicle [11]. Based on direct impinging jet concept on the hot-side, the module produced approximately 1960 µW from a 58°C waste stream. Singh et al. [20] applied swirl to a heat stream at 60oC and produced an enhanced power of 3056 µW from a single TEG cell.

These cases indicate that TEG modules are continuously developed as an auxiliary system for fuel cell systems to enhance its overall energy efficiency. However, to achieve optimal power outputs for low grade waste heat from PEM fuel cells, further evaluation on geometry and configurations of the heat transfer devices within the module must be taken, relative to the operation and constraints if the fuel cell application. Computational heat transfer analysis is a viable approach for this purpose.

There are limited studies in computational numerical modelling works for fuel cell energy recovery whereas it is an important tool for progressive design in thermal engineering. Mohamed et al. [12] developed a numerical model of a single cell TEG module for FCV energy recovery. The model was applied to predict the outputs for series and parallel power train configurations with variations to the waste heat temperature (WHT) and vehicle speed. It was concluded that at 100 kmh-1 FCV speed, the parallel configuration generates 50% more power than the series configuration. Simulation models were developed by Gao et al. [21, 22] for heat recovery of high temperature PEM fuel cells to identify the optimal configurations for the module and they stated that superior outputs can be obtained by focusing on designing highly effective compact heat exchangers. Relatively, advanced numerical modelling with coupled fluid dynamics and thermoelectric models were developed by Högblom and Andersson [23] and Chen et al. [24]. These models enable simultaneous heat transfer and electrical power prediction as a function of temperature across the TEG module.

Generation of electrical power from low temperature waste heat streams, such as from an open-cathode PEM fuel cell, is viable only if the cooling mode requires no parasitic power consumption. Due to low temperature differences across the TEG cells, a high power density should not be expected. Therefore, integrating TEG modules with other waste heat utilization method would improve the overall efficiency, such as for reactant preheating.

Using the waste heat to preheat the fuel cell reactants have been proposed in limited studies as listed in Table 1. Preheating the hydrogen stream by 10°C have shown stack power increments by approximately 8% in an open-loop hydrogen supply configuration [25]. This was generally achieved due to the increase in Nernst potential as the stack temperature increases. The increase in hydrogen temperature also led to relative increase in its partial pressure across the anode, producing greater diffusion through the electrode assembly and higher electrochemical kinetic reactions. Zhang et al. [26] also applied hydrogen preheating using a shell and tube heat exchanger design with corrugated knotted tubes.

An 8.1% fuel cell power increase was obtained from a waste heat stream of approximately 70°C. Relatively, Nguyen et al. [27] explored the possibility of preheating reactant air of a PEM fuel cell stack. The numerical model predicted the temperature increase under varying conditions and was validated using a theoretical model.

Table 1 - Studies on PEM fuel cell WHR for reactants preheating

References	**Mohamed and Kamil [25]**	**Zhang et al. [26]**	**Nguyen et al. [27]**
Heat Recovery Method	Finned + Multi Tube Pass Heat Exchanger	Shell And Tube + Corrugated Knotted Tubes	Heat Exchanger + External Electric Heater
Application	Hydrogen Preheating of PEMFC	Hydrogen Preheating	Air Preheating of PEMFC
Heat Source	PEMFC Waste Heat	Fuel Cell Engine PT100	PEMFC Waste Heat
Heat Source Temperature	40 – 45 °C	-30 - +70 °C	-50 - +30 °C
Methodology	Experimental + Theoretical Model	Experimental + Numerical Model	Numerical Model + Theoretical Model
Power Increment	8-10 %	8.1%	N/A
Waste Heat utilization	3 - 6%	N/A	N/A

The integration of TEG technology and hydrogen preheating relative to WHR of a PEM fuel cell is a new concept to be explored and can be relatively referred as Combined Heat and Power (CHP) approach. The TEG cells directly produce electrical power and the hydrogen absorbs the waste heat to increase its supply temperature. Consequently, the increase in hydrogen temperature also leads to enhanced power outputs from the fuel cell stack. Therefore, it is hypothesized that higher overall fuel cell system efficiency can be obtained.

This manuscript presents numerical computational analysis of an integrated heat regenerator (IHR) system concept consisting of TEG cells and hydrogen preheater designed for a mini 2 kW powered FCV. The fuel cell type is an open cathode PEM fuel cell where its actual electrical and thermal outputs are mapped and applied as boundary conditions. The IHR design concept consists of two sections – a compact heat exchanger section for hydrogen preheating and a TEG module section with embedded heat pipes and cooling fins. Three IHR design options were proposed, modelled and analysed. The objectives of the numerical modelling are to evaluate the outputs of the three designs and identify the related engineering issues towards producing improved designs in the future. The results were validated with the outputs of a theoretical model developed specifically for the IHR system. The main parameters studied were the hydrogen preheating degree, the fuel cell power output enhancement, the TEG temperature profiles and power outputs, as well as the waste heat utilization. The proposed IHR concept is novel and the presented contents of this manuscript may lead to intensive studies on advanced IHR designs for practical FCV application. In the future, it is envisioned that the IHR would be an integral auxiliary system for mobile and stationary fuel cell systems to improve the overall system efficiency.

NOMENCLATURE

v_{WH}	Kinematic Viscosity Of Air (m^2/s)
v_{H^2}	Kinematic Viscosity Of Hydrogen (m^2/s)
u_{H^2}	Fuel Cell Exhaust Air Velocity (m/s)
u_{WH}	Fuel Cell Vehicle Cruising Speed (m/s)
u_{H^2}	Hydrogen Inlet Velocity (m/S)
h_i	Convection Coefficient Of The Tube Side ($W/m^2\,K$)
h_{FCV}	Convection Coefficient At The Cooling Heat Sink Due To The FCV Motion ($W/m^2\,K$)
h_{WH}	Convection Coefficient Of Waste Heat Air ($W/m^2\,K$)
h_o	Convection Coefficient At The Air Side (Fin Side) ($W/m^2\,K$)
U	Overall Heat Transfer Coefficient For The Heating Heat Exchanger($W/m^2\,K$)
$\dot{Q}_{\text{actual}}$	Actual Heat Transfer (W)

$\dot{Q}_{max}$	Maximum Possible Heat Transfer (W)
$\dot{Q}_{\mathrm{T.c}}$	Total Heat Transfer Rate Through the Heat Exchanger (W)
$\dot{Q}_{H2}$	Preheating Rate Of Hydrogen (W)
Nu_{H2}	Hydrogen Nusselt Number
Nu_{WH}	Waste Heat Nusselt Number
ε	Effectiveness
NTU	Number Transfer Unit
Pr	The Prandlt Number
Re_{H^2}	Hydrogen Reynolds Number
Re_{WH}	Waste Heat Air Reynolds Number
T_h	TEG Hot Side Temperature From CFD (°C)
ΔT_{TEG}	TEG Surfaces Temperature Difference (°C)
T_{WH}	Waste Heat Temperature (°C)
T_{FCV}	Fuel Cell Vehicle Cruising Temperature (°C)
$T_{TEG,c}$	TEG Cold Surface (°C)
$T_{TEG,h}$	TEG Hot Surface (°C)
$T_{H2.\ in}$	Hydrogen Inlet Temperature (°C)
ΔT_{H2}	Hydrogen Temperature Difference (°C)
T_{FC}	Fuel Cell Exhaust Air Temperature (°C)
D_i	Inner Diameter Of The Tube (m)
OCV	Open Circuit Voltage (V)
$R_{T.C}$	Total resistance in the heat exchanger (K/W)
R_{TEG}	Resistance for TEG (K/W)
${}^{n}_{12}R_{TEG}$	Total resistance for 12 TEG in parallel (K/W)
${}^{n}_{4}R_{Heat\ pipe\ //\ Fin}$	Total resistance for 4 set of 2 heat pipes and 50 fin heat sink (K/W)
$R_{Heat\ sink}$	Total resistance for the heatsink (K/W)
R_{copper}	Resistance for copper (K/W)
R_{Fin}	Resistance for fin (K/W)
t_{copper}	Copper plate thickness (m)
$L_{Heat\ pipe}$	Heat pipe length (m)
L_{Fin}	Fin length (m)
t_{TEG}	TEG thickness (m)
$L_{Heat\ sink}$	Heat sink length (m)
$A_{Heat\ sink}$	Area heat sink (m^2)
A_{TEG}	Area TEG (m^2)
A_{Fin}	Area fin (m^2)
A_s	Total heat transfer surface area (m^2)
A_{copper}	Area copper plate (m^2)
$A_{Heat\ pipe}$	Area heat pipe (m^2)
$k_{Aluminium}$	Thermo conductivity aluminum $(W/m.K)$
$k_{Bismuth\ telluride}$	Thermo conductivity bismuth telluride $(W/m.K)$
k_{copper}	Thermo conductivity copper $(W/m.K)$
k_{H^2}	Hydrogen thermal conductivity $(W/m.K)$
$\dot{m}_{FC}$	Fuel cell exhaust air mass flow rate (kg/s)
$\dot{m}_{H2}$	Hydrogen mass flow rate (kg/s)
μ_{WH}	Waste heat utilization factor (%)
μ_{PFC}	PEMFC power increment from hydrogen preheating (%)
$P_{el,FC}$	Fuel cell electrical power output (W)
$\Delta P_{el,FC}$	PEMFC power increment from hydrogen preheating (W)
$P_{th.\ FC}$	Fuel cell thermal power output (W)
P_{TEG}	TEG electrical power (W)
$C_{p.H2}$	Heat capacity of hydrogen
$C_{P.min}$	Smallest heat capacity rate between the hydrogen and waste heat streams ($J{\cdot}kg^{-1}{\cdot}°C^{-1}$)
H_{fin}	Height of the fin (m)
α	Seedback coefficient ($mVK{-}1$)
I_{SC}	Short circuit current (A)

ABBREVIATIONS	
CHP	Combined Heat and Power
FCV	Fuel Cell Vehicle
IHR	Integrated Heat Regenerator
OCV	Open Circuit Voltage
ORC	Organic Rankine Cycle
NTU	Number of Transfer Units
PEM	Polymer Electrolyte Membrane
TEG	Thermoelectric Generator
WHR	Waste Heat Recovery
WHT	Waste Heat Temperature

2. Methodology

The methodology is divided into four sections – the IHR system functionality, the output analysis, the theoretical model development and the computational numerical model development.

2.1 IHR System Design and Operation

A mini FCV developed for research purpose was driven by a 2 kW open-cathode PEM fuel cell stack. The IHR system is located downstream at the exit of the air stream from the stack. The IHR functions as a CHP system where waste heat from the fuel cell is regenerated for two purposes. The first is to preheat hydrogen before it enters the stack and the second is for direct electrical power generation using TEG cells. Fig. 1 shows the overview of the IHR system. The main components of the system are open-cathode PEM fuel cell stack, hydrogen supply, TEG cells, as well as finned heat exchangers for heat absorption and removal. The fuel cell stack used in the FCV is Horizon H-2000 with specifications as listed in Fig. 2. The TEG used is the design model is made of Bismuth Telluride semi-conductor with 60 mm width, 60 mm height and 6 mm thickness [27, 28].

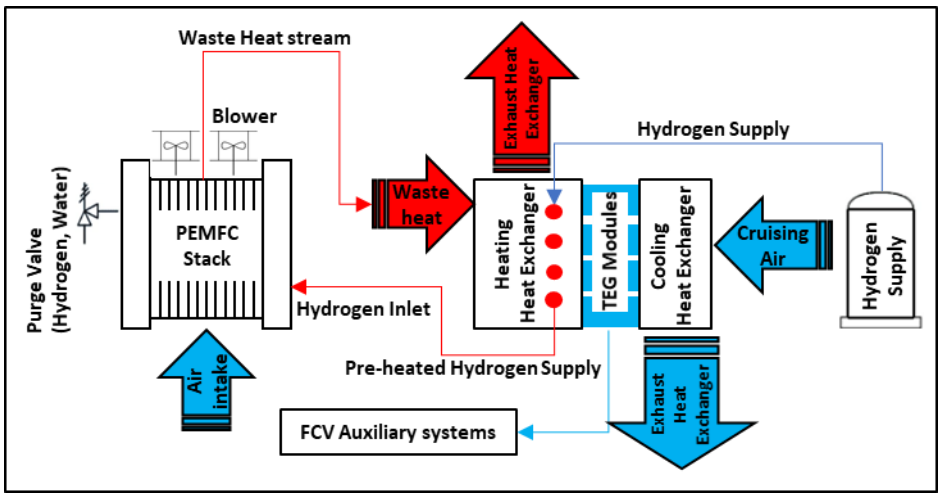

Fig. 1 - Overview of the IHR system for WHR from an open-cathode PEM fuel cell stack

Specification	Details
Model / Fuel cell type	Horizon H2000/ PEM
No. of cells / Cooling	48 / Air
Rated max. power	2000 W
Rated max. performance	28.8 V @ 70 A
Max. stack temperature	65 °C
Flow rate at max. output	26 L/min
Dimensions (Height x width x length)	(35 x 30.3 x 18.3) cm

Fig. 2 - Specifications for Horizon H2000 PEM fuel cell stack

The fuel cell stack functions to generate electrical power from the electrochemical reactions between hydrogen and oxygen, producing heat and water vapour as by-products. Air flows into the stack through the use of negative pressure fans (suction) at the back of the stack for oxygen supply as the reactant as well as heat removal. The heated air stream temperature is dependent on the thermal power generated by the stack which is relative to the electrical power discharge of the stack. The stack waste heat within the air stream is normally rejected directly to the surrounding. In this work, the IHR was developed with multi-pass finned-tube heat exchangers to capture a portion of the low-grade waste heat (stream temperature less than 100°C) and utilize it mainly as a source for hydrogen preheating.

The waste heat stream impinging on the heat exchanger fins increases the heat exchanger surface temperature and the heat is then transferred to one side of the TEG cells surfaces. Thus, one side of the TEG surface is continuously heated by the waste heat stream. As the heat flows through the TEG cells due to temperature difference between the cell surfaces, free electros are excited within the semi-conductor material and generates electrical power proportionate to the temperature difference (heat transfer rate) between the TEG surfaces. To achieve a significant amount of electrical generation, one side of the TEG cell needs to be actively cooled. In this IHR design for a mini FCV, the cooling air stream is obtained from the movement of the vehicle through the use of finned heat sinks that is connected to the TEG cold-side using heat pipes for effective heat transfer. The cooling heat sinks extracts the heat from the TEG at a rate relative to the cruising speed of the FCV.

The Horizon H-2000 stack has a rated maximum power of 2000 W. The main boundary condition for the design model of the IHR designs is the waste heat air stream temperature. The hot air temperatures ranged between 29°C to 51°C was based on 500 W to 2000 W of stack power outputs, where stack exhaust temperatures was mapped with stack power capacity, which was experimentally measured from the exit air of the PEMFC at different stack loads [12, 17]. As this hot air are from the exhaust stacks it acts as the WHT which would later be absorb by the IHR system at the heating exchanger side. Adopted from previous study the cooling air velocity was fixed at the design cruise speed of the FCV of 36 km/h, with an ambient temperature of 30 °C ([12], [17]). The mass flowrates of hydrogen inlet was acquired from Mohamed et. al [25] with constant temperature (30°C) from the hydrogen supply tank. Table 2 lists the values of the parameters (extracted from Mohamed et. al [12], [17], [25]) applied in this study as initial and boundary conditions for the numerical design evaluation.

Table 2 - Domain parameters for the IHR system for PEMFC

Domain/ streams	Parameters	Unit	Symbol	Stack Power (W)			
				500	1000	1500	2000
FC Stack	Mass Flow Rate	kg/s	$\dot{m}_{FC}$	2.81	3.02	3.22	3.40
Waste Heat	Velocity	m/s	u_{FC}	2.48	2.73	2.98	3.23
Stream	Temperature	°C	T_{FC}	29.23	36.53	43.83	51.13
Hydrogen	Mass Flow Rate	kg/s	$\dot{m}_{H2}$	9.04E-06	1.81E-05	2.71E-05	3.62E-05
Inlet	Velocity	m/s	u_{H2}	0.49	0.97	1.46	1.94
	Temperature	°C	T_{H2}	23	23	23	23
Cooling Stream	Cruising Velocity	m/s	u_{FCV}	10	10	10	10
	Temperature	°C	T_{FCV}	30	30	30	30

Three IHR design concepts with multi-pass finned-tubes for hydrogen preheating and finned-heat pipes for TEG cell cooling were developed and modelled for performance analysis using computational fluid dynamics (CFD). Overall, all the designs consist of multi-pass hydrogen supply tubes, plate-finned heat exchanger attached to a base copper plate, TEG cells attached to the base copper plate, heat pipes that connects the TEG cells to the cooling heat sinks, and plate-finned heat sinks for TEG cooling. Figs. 3a to 3f shows the configurations of Designs 1 to 3. All designs have smaller frontal areas than the PEM fuel cell stack size (35 cm height and 30 cm width).

Table 3 lists the specifications of the designs. Design 1 is the reference design where the hydrogen tube was designed with a 6-pass configuration, leading to a larger heat exchanger area and allowing 12 TEG cells to be positioned at the base copper plate. The cooling heat sinks were positioned away from the heating heat exchangers to effectively capture the air stream from the vehicle movement. However, heat pipes with greater length were needed. Designs 2 and 3 reduced the number of hydrogen tube passes to 4 as an approach to develop a more compact and lightweight IHR system. The reduction in the heating heat exchanger size reduced the number of TEG cells that can be mounted to the base plate to 6 cells. Designs 2 and 3 also have similar 15 units of heat pipes. However, Design 3 has a different heat pipe-fin assembly to Design 2. As shown in Figs. 3c and 3d, Design 2 has 15 heat pipes in 1 set of 50 fin heat sinks with a similar size for each fin. Compared with design 3, consist of 3 heat pipes in 1 set of 10 fin heat sinks and, 2 sets of 6 heat pipes of 20 fin heat sinks. This is to reduce the IHR size but to maintain 10 fin heat sinks for 3 heat pipes.

The main output criteria of the IHR is to preheat the hydrogen by a minimum of 10°C which would lead to a fuel cell power enhancement by approximately 8% [25]. Due to the low operating temperature of the stack (at 60°C), higher hydrogen temperatures might cause severe membrane dehydration that damages the electrode assembly.

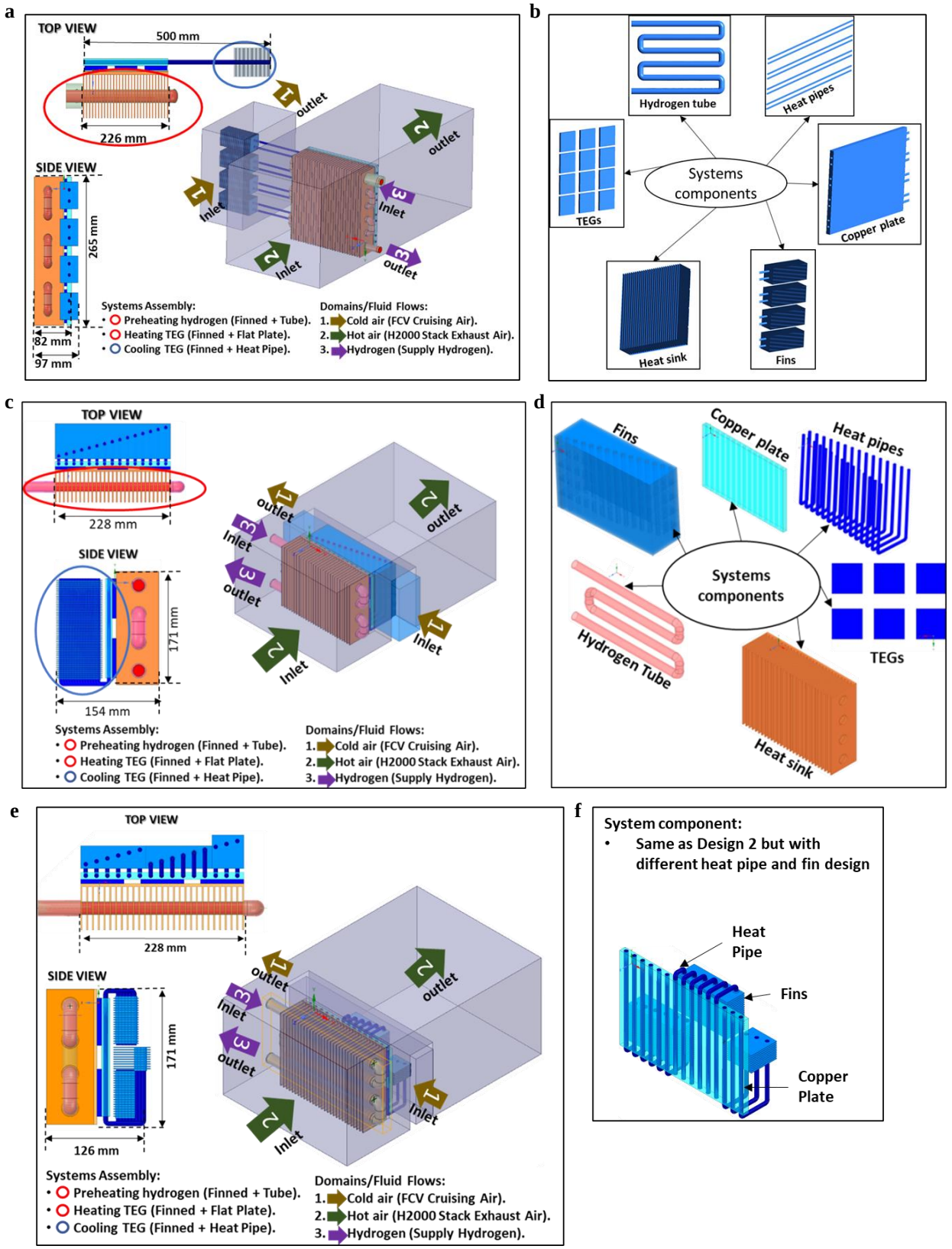

Fig. 3 - Heating and cooling heat exchanger configurations and specifications. (a) Design 1 assembly; (b) Design 1 components; (c) Design 2 assembly; (d) Design 2 components; (e) Design 3 assembly; (f) Design 3 components

Table 3 – IHR heat exchanger designs parameters

Design Parameters	Unit	Design 1	Design 2	Design 3
System Size (Width x Height x Length)	**(m)**	0.500 x 0.265 x 0.097	0.228 x 0.171 x 0.154	0.228 x 0.171 x 0.126
Heating Surface Area	(m^2)	1.06	0.69	0.69
Cooling Side Surface Area	(m^2)	0.775	1.56	0.281
No. Tubes Pass	-	6	4	4
No. of Fins on Heatsink		29	29	29
No. Heat Pipes	-	8	15	15
No. Heat Sink Fins	-	4 sets of 50 fin heat sinks	1 set of 50 fin heat sinks	2 sets of 20 fin heat sinks 1 set of 10 fin heat sinks
TEG Cells	-	12	6	6

2.2 Performance Analysis

The IHR designs were evaluated on the hydrogen temperature difference, hydrogen heat absorption, TEG power generation, power enhancement of PEMFC and waste heat utilization. The numerical model provided temperature values for the hydrogen stream as well as the surface temperatures of the TEG cells under variable waste heat stream temperatures. These temperatures were then translated to calculate the rate of heat absorption by the hydrogen stream as well as the TEG electrical power outputs. To predict the fuel cell power enhancement due to hydrogen preheating, a simplified method was used by referring to the results of a previous study by Mohamed and Kamil [25] who mapped the enhancement of a PEM fuel cell stack power output against the hydrogen preheating degree. Experimental data from [25] were mapped, as shown in Fig. 4, and a correlation was obtained (Eq. 1) as reference to calculate the fuel cell enhancement for this study.

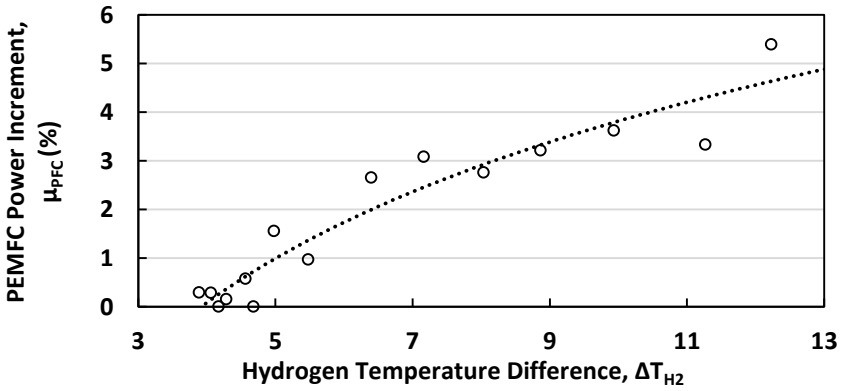

Fig. 4 - PEMFC power output increment per degree of fuel preheating (extracted from [25])

From the exponential profile in Fig. 4, the percentage of PEMFC power increment relative to the degree of preheated hydrogen temperature can be expressed as

$$\mu_{PFC} = (0.569 \cdot \Delta T_{H2}) - 1.9355 \quad (\%) \tag{1}$$

where ΔT_{H2} is the inlet and outlet temperature difference of the hydrogen stream at the heating heat exchanger, which is then used to predict the PEMFC power output enhancement,

$$\Delta P_{el,FC} = P_{el,FC} \cdot \mu_{PFC} \quad (W) \tag{2}$$

where $P_{el,FC}$ is the nominal electrical power output from the fuel cell (500 W to 2000 W).
From the hydrogen temperature difference, the preheating rate of hydrogen is

$$\dot{Q}_{H2} = \dot{m}_{H2} \cdot C_{p.\,H2} \cdot (\Delta T_{H2}) \ (W) \tag{3}$$

The mass flow rate of hydrogen relative to the stack power output, $\dot{m}_{H2}$ and the heat capacity of hydrogen, $C_{p,H2}$ is listed in Table 2.

The waste heat utilization factor, μ_{WH} is the ratio of combined heating rate of hydrogen preheating and TEG power generation, P_{TEG} to the thermal power generated from the stack, $P_{th.FC}$ relative to the fuel cell power output.

$$\mu_{WH} = \frac{\dot{Q}_{H2} + \dot{Q}_{\mathrm{T.c}}}{P_{th.\ FC}} \tag{4}$$

In this work, the $P_{th,FC}$ is assumed similar in magnitude to the electrical power generated (a 50% energy conversion efficiency assumption).

2.3 Theoretical Model

The theoretical model of the IHR was developed for the purposes of obtaining the geometrical guidelines for the design as well as to validate the CFD results. The model is divided into two parts. The first part is for the hydrogen preheating heat exchanger while the second part is for the TEG cells, inclusive of the cooling heat sink.

The sizing of the hydrogen preheating heat exchanger is influenced by the number of fins, number of tube passes, length of the fins and length of the tubes. The effectiveness-NTU method, as in Eqns. (5) to (14), was applied to predict the hydrogen exit temperature from a fixed operating condition and heat exchanger geometrical parameters.

The Reynold numbers for the hydrogen and waste heat (air) can be calculated from

$$Re_{H^2} = \frac{u_{H^2}.\ D_i}{v_{H^2}} \tag{5}$$

$$Re_{WH} = \frac{u_{WH}.\ H_{fin}}{v_{WH}} \tag{6}$$

where Re is the Reynold number, u is velocity, D_i is the inner diameter of the tube which is 0.01704 m, H_{fin} is the height of the fin (refer to Fig 3) and v is the kinematic viscosity of hydrogen and air at their respective initial temperatures.

Then, the Nusselt number is determined for both streams,

$$Nu_{H2} = \frac{h_i.\ D_i}{k_{H^2}} \tag{7}$$

$$Nu_{WH} = 0.228 \cdot \mathrm{Re}_{\mathrm{WH}}^{0.731}.\,\mathrm{Pr}_{\mathrm{WH}}^{0.33} \tag{8}$$

where h_i is the convection coefficient of the tube side, k_{H2} is the thermal conductivity of hydrogen and Pr_{WH} is the Prandtl number of the waste heat air stream. Since hydrogen flow in the tube is laminar and assumed to be fully developed flow hence the value for Nu_{H2} is 4.36 for a constant heat flux case [29].

The overall heat transfer coefficient, U, for the heating heat exchanger is

$$\frac{1}{U} \approx \frac{1}{h_i} + \frac{1}{h_o} \tag{9}$$

where h_o is the convection coefficient at the air side (fin side), which is 45.79 (W/m^2K).

The actual rate of heat transfer is a product of effectiveness of heat exchanger and the maximum heat transfer rate. The prediction on the value of preheated hydrogen outlet temperature can be obtained using the heat exchanger effectiveness definition, where the predicted temperature was used to validate the simulation results.

$$\dot{Q}_{actual} = \varepsilon \dot{Q}_{max} \tag{10}$$

The effectiveness, ε, is related to the NTU of the heat exchanger,

$$\varepsilon = 1 - exp(-NTU) \tag{11}$$

$$NTU = \frac{U \cdot A_s}{C_{P,min} \cdot \dot{m}} \tag{12}$$

where NTU is the dimensionless number of transfer units of the heat exchanger, A_s is total heat transfer surface area of the heat exchanger and C_{min} is the smallest heat capacity rate between the hydrogen and waste heat streams.
The maximum possible heat transfer, $\dot{Q}_{max}$, is dependent on the maximum temperature difference of the hydrogen preheating process,

$$\dot{Q}_{max} = \dot{m}_{H2} \cdot C_{p.\,H2} \cdot (T_{WH} - T_{H2.\,in}) \tag{13}$$

$\dot{m}_{H2}$ is mass flow rate of hydrogen supply, $C_{p,H2}$ is the specific heat capacity of hydrogen, T_{WH} is the WHT and $T_{H2,in}$is the inlet temperature of hydrogen.
The preheated temperature for hydrogen $T_{H2,out}$ can be obtained from

$$T_{H2.\,out} = T_{H2.\,in} + \frac{\dot{Q}_{\text{actual}}}{\dot{m}_{H2} \cdot C_{H2}} \tag{14}$$

For the prediction of the TEG surface temperatures, a one-dimensional thermal resistance analysis was applied across the fins of the heating heat exchanger, the TEG cells and the cooling heat sink. Fig. 5 shows an example of the thermal resistance network for Design 1 which is a combination of parallel and series resistance configuration relative to the heat flow direction from the waste heat stream towards the cooling air stream. The resistance for the multiple components (TEGs, heat pipes, fins) are in parallel conduction. The thermal resistance with parallel resistance can be simplified to a series circuit as shown in Fig. 6.
The TEG surface can be predicted using

$$T_{TEG,h} = T_{Base} - \frac{\dot{Q}_{\text{T.c}}}{R_{copper}} \tag{15}$$

$$T_{TEG,c} = T_{TEG,h} - \frac{\dot{Q}_{\text{T.c}}}{{}^{n}_{12}R_{TEG}} \tag{16}$$

where $T_{TEG,c}$ is the TEG cold surface and $T_{TEG,h}$ is the hot surface temperature. T_{Base} is the heatsink base temperature, while $\dot{Q}_{\text{T,c}}$ is the total heat transfer rate through the heat exchanger assembly,

$$\dot{Q}_{\text{T,C}} = \frac{T_{WH} - T_{FCV}}{R_{T,C}} \tag{17}$$

where $R_{T,C}$ is the total resistance in the heat exchanger (as in Fig. 6),

$$R_{T.C} = R_{Heat\ sink} + R_{Copper} + {}^{n}_{12}R_{TEG} + R_{Copper} + {}^{n}_{4}R_{Heat\ pipe\ //\ Fin} \tag{18}$$

where $R_{Heat\ sink}$, R_{Copper}, ${}^{n}_{12}R_{TEG}$, ${}^{n}_{4}R_{Heat\ pipe\ //\ Fin}$ are the total resistance for the heatsink, copper plate, combined heat pipe and fins. ${}^{n}_{4}R_{Heat\ pipe\ //\ Fin}$ are the sum of $R_{Heat\ pipe}$ and $R_{Heat\ sink}$ from the parallel thermal resistance accounting the actual number of fins and heat pipes.

$$R_{copper} = \frac{t_{copper}}{k_{copper} A_{copper}} \tag{19}$$

$$R_{Heat\ pipe} = \frac{L_{Heat\ pipe}}{k_{copper} A_{Heat\ pipe}} \tag{20}$$

$$R_{Fin} = \frac{L_{Fin}}{k_{Aluminium} A_{Fin}} + \frac{1}{h_{FCV} A_{Fin}} \tag{21}$$

$$R_{TEG} = \frac{t_{TEG}}{k_{Bismuth\ telluride} A_{TEG}} \tag{22}$$

$$R_{Heat\ sink} = \frac{L_{Heat\ sink}}{k_{Aluminium} A_{Heat\ sink}} + \frac{1}{h_{WH} A_{Heat\ sink}} \tag{23}$$

where h_{WH} is the heat transfer coefficient for the fuel cell waste heat and h_{FCV} is the heat transfer coefficient at the cooling heat sink due to the FCV motion.

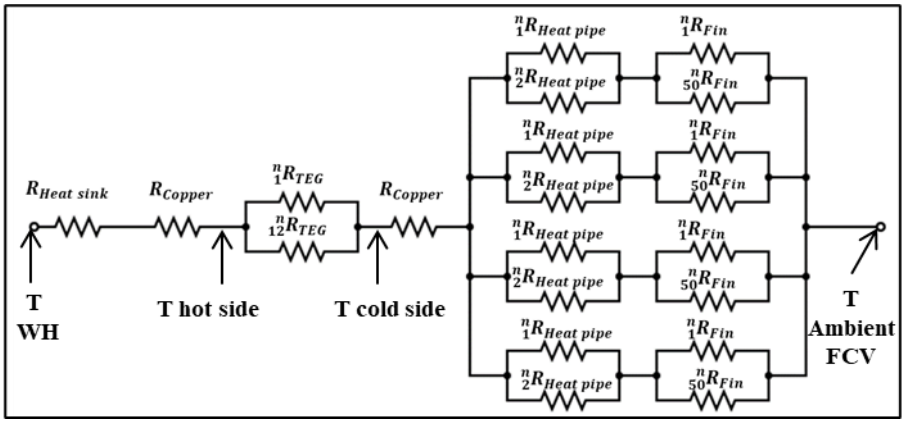

Fig. 5 – Example of thermal resistance network for IHR Design 1

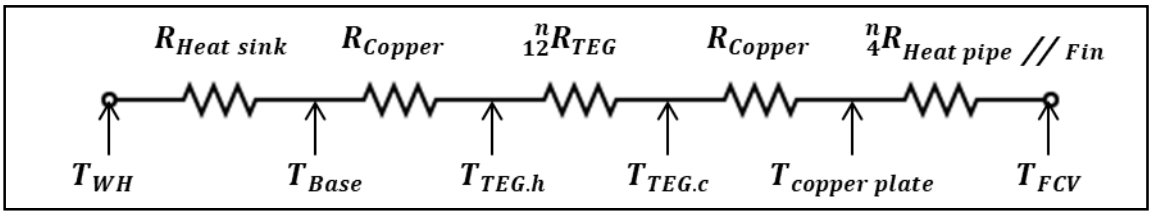

Fig. 6 – Simplified thermal resistance circuit for Design 1

The calculation for the power output of the TEG cells was based on the method by Mohamed et al. [12]. The peak power output that can be obtained from the power potential of a TEG is theoretically 25% from the optimum TEG power that occur when the short circuit current is multiplied by the open circuit voltage. Both parameters are dependent on the surface temperatures of the TEG cell. Therefore, the TEG power output was predicted using Eqs. 24 to 26.

$$P_{TEG} = \frac{1}{4} . I_{SC} . OCV \tag{24}$$

$$OCV = \alpha . \Delta T_{TEG} \tag{25}$$

$$I_{SC} = (1.44 . T_{h.}) - 48.3 \tag{26}$$

The I_{SC} is defined as the short circuit current obtained when the cell voltage is zero, while OCV is the open circuit voltage that occurs when the cell current is zero. The value of the hot side and cold side TEG surfaces from the simulation was used calculate the temperatures difference for the TEG module, ΔT_{TEG} and the OCV. The hot side TEG surface temperature, $T_{h.}$ from the simulation was used to calculate $I_{SC.}$ The Seebeck coefficient, α, is equal to 24.7 mVK^{-1} [12] that shows the constant temperature thermoelectric potential of the semiconductor material.

2.4 Numerical Model

Computational numerical modelling analysis of the designs allow a more detail heat transfer interactions to be captured across the IHR compared to the one-dimensional theoretical model. All three IHR heat exchangers were simulated on ANSYS Fluent 2021 R1 CFD software. There are three fluid domains in the simulation:

(i) waste heat air flow from the PEM fuel cell - the initial velocities, flow rates ($u_{WH}, \dot{m}_{WH}$) and temperatures (T_{WH}) were varied based on the electrical power generated from the stack (500 W to 2000 W).

(ii) ambient air at the cooling heat sink – the FCV velocity was constant at a cruising speed of 35 kmh^{-1} (10 m/s) while the air temperature is constant at an ambient of 30 °C,

(iii) hydrogen stream from the supply tank - the initial velocities, flow rates (u_{H2}, $\dot{m}_{H2}$) and temperatures (T_{H2}) were varied based on the stack electrical power generation (500 W to 2000 W).

The values of these boundary conditions for the simulations are as listed in Table 2.

The flow regimes inside the hydrogen tubes is laminar with a maximum Reynolds number of approximately 300 due to the small quantity of hydrogen mass flow rate needed for a fuel cell power output between 500 W to 2000 W. However, the Reynolds number across the finned-tube and finned-heat pipe at the heating and cooling heat exchanger exceeded 30000 and an impinging air jet on the fins of the heat exchanger and heat sink would produce streamlines with non-laminar profiles. Therefore, external convection computations require the use of turbulence model. The 3-dimensional models were simulated under steady-state heat transfer with the assumption of incompressible stream for both air and hydrogen. The heat pipe model was also simplified as solid copper rods due to the complexity of modelling the boiling and condensation of the heat pipe fluid within the heat exchanger model.

The complex geometry of the full IHR model with multiple thin fins (0.2 mm thickness) caused a poor quality of hexahedral and tetrahedral elements on the fin surfaces and on the wall surfaces near the fin area. To compensate this, a very fine element size (0.01 mm) was applied on the fin-fluid boundaries. This produced approximately 7 million elements on a single full assembled model.

The realizable k-ε turbulence model was adopted for the flow regime model and energy model heat transfer. The Pressure-based coupled algorithm was used for the coupling of pressure and velocity as to overcome the complex meshing and a second-order upwind scheme was considered for the spatial discretization of equations of pressure, continuity, momentum, turbulent kinetic energy, and turbulent dissipation rate [30], [31].

Continuity equation,

$$\nabla \cdot (\rho \vec{u}) = 0 \tag{27}$$

Momentum equation,

$$\nabla \cdot (\rho \vec{u} \vec{u}) = -\nabla P + \mu \nabla^2 \vec{u} + \rho \vec{g} \tag{28}$$

Energy equation,

$$\nabla \cdot \left(C_P \rho \vec{u} T \right) = k \nabla^2 T \tag{29}$$

where *u, P, T, μ, g* and *ρ* are the velocity, pressure, temperature, fluids viscosity, gravity and density respectively. For impinging airstreams jet through a heatsink with turbulent flow regime, a Reynolds Averaged Navier-Stokes (RANS) was used to solve two turbulence equations with a realizable k-ε [26, 32] The turbulence transport equations are expressed as, for $k_{Turbulant}$,

$$\frac{\delta k}{\delta x_j} \cdot \left(\rho \cdot \bar{u}_j \right) = \frac{\delta}{\delta x_j} \cdot \left(\frac{\mu_t}{\sigma_k} \cdot \frac{\delta k}{\delta x_j} \right) + \mu_t \left(\frac{\delta \overline{\mu}_i}{\delta x_j} + \frac{\delta \overline{\mu}_j}{\delta x_i} \right) \frac{\delta \overline{\mu}_i}{\delta x_j} - \rho \cdot \varepsilon \tag{30}$$

For ε,

$$\frac{\delta \varepsilon}{\delta x_j} \cdot \left(\rho \cdot \overline{u}_j \right) = \frac{\delta}{\delta x_j} \cdot \left(\frac{\mu_t}{\sigma_\varepsilon} \cdot \frac{\delta \varepsilon}{\delta x_j} \right) + C_1 \mu_t \frac{\varepsilon}{k} \left(\frac{\delta \overline{\mu}_i}{\delta x_j} + \frac{\delta \overline{\mu}_j}{\delta x_i} \right) \frac{\delta \overline{\mu}_i}{\delta x_j} - C_2 \cdot \rho \cdot \frac{\varepsilon^2}{k} \tag{31}$$

where k turbulent kinetic energy, ε turbulent dissipation and the constants are C_1=1.44, C_2=1.92, C_μ= 0.09, σ_k= 1, σ_ε=1.3. Here i, j = 1, 2 and 3 represent 3-D directions, respectively [26], [32]. The CFD setup is summarized in Table 5 and the material properties in Table 4. The convergence criteria were solved with the highest residue of 10^{-3} for continuity, momentum, $k_{Turbulant}$, ε, and lowest 10^{-8} for energy.

Table 4 - Material properties

Properties	Unit	Symbol	Material					
			Copper Flat Plate/ Heat Pipe	Glass Mineral Wool Insulator	Air Hot Stream/ Cold Stream	Hydrogen	TEG Bismuth Telluride	Aluminium Plate Fins/ Heatsink
Density	*kg/m^3*	ρ	20	20	1.059	0.08189	7730	2719
Specific Heat Capacity	*J/kg.K*	C_p	381	1030	1007	Piecewise polynomial	157.35	871
Thermal Conductivity	*W/m.k*	k	387.6	0.35	0.02808	0.1672	1.2	202.4

Table 5 - Parameters for CFD setup

Parameters	Selection
Solver	
Type	Coupled, Pressure- Based
Velocity Formulation	Absolute
Models	
Energy	On
Viscous	Realizable K- epsilon
Solution Methods	
Momentum	2nd order upwind
Turbulent Dissipation Rate	2nd order upwind

The additional and summarized assumptions adapted for the numerical model are as follows:

(i) The model incorporates conduction and convective heat transfer. The effect of radiation is neglected.
(ii) The system is simulated under a steady state condition, where the density of all the fluids streams are kept constant for an incompressible flow model.
(iii) There is no heat transferred from the system to the surroundings. The heat is only released via the cruising cold air.
(iv) The heat transferred within the heat pipe is by conduction through the length of solid copper rod. Neglecting the complex boiling and condensation fluid model inside the heat pipe within the IHR system.
(v) All three fluids streams are flown in separated domain, where a single phase modelled is used.
(vi) All the fluids are steady, turbulent viscosity is isotropic and flown in a uniform velocity.

3. Results & Discussion

The results are discussed based on the three IHR system designs performance following the consecutives modelling validation and objectives.

(i) CFD model validation by comparing the output parameters between the simulation and theoretical results.
(ii) The hydrogen preheating capability from the IHR system on varied PEMFC power.
(iii) The predicted Fuel Cell Power Enhancement due to Hydrogen Preheating.
(iv) The simulated TEG temperature profiles.
(v) The predicted TEG power output.
(vi) The amount of utilize waste heat from PEMFC exhaust.

3.1 Validation of CFD Model

The main parameters from the simulations are the hydrogen exit temperature from the heat exchanger and the surface temperatures of the TEG cells (hot and cold sides). Figs. 7a, b and c shows the comparison between the CFD model and theoretical results of the temperatures. In general, Figs. 7 and 8 demonstrated the temperatures of hydrogen outlet and TEG surfaces had increased in a linear profile proportionately to the fuel cell nominal power output, relative to the increase in WHT. This is due to the greater available source of waste heat energy. As the fuel cell electrical power output generated is proportional to the amount of thermal power produced, a rise on fuel cell power operation provides higher heat source for the IHR system to absorb. In return ascending heating power is available for the system to transfer it to hydrogen stream and TEG surfaces. Only a small difference was registered for all parameters. Further analysis on the

percentage differences of each parameter in Fig. 8 is not higher than 5%. Both models for Design 1 and 3 are in high agreement (less than 2% difference) whereas the models for Design 2 have a higher difference. The comparisons indicate a good confidence level of the heat exchanger CFD models, where acceptable simulations using Ansys-Fluent turbulence model usually have less than 10 % maximum difference [33].

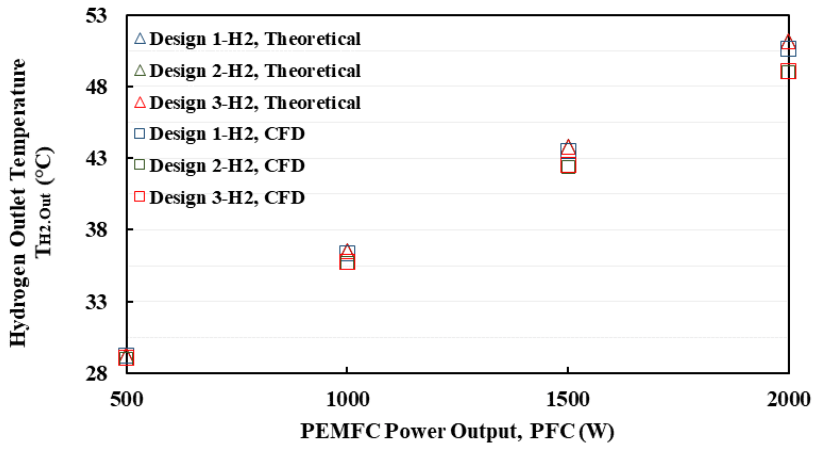

(a)

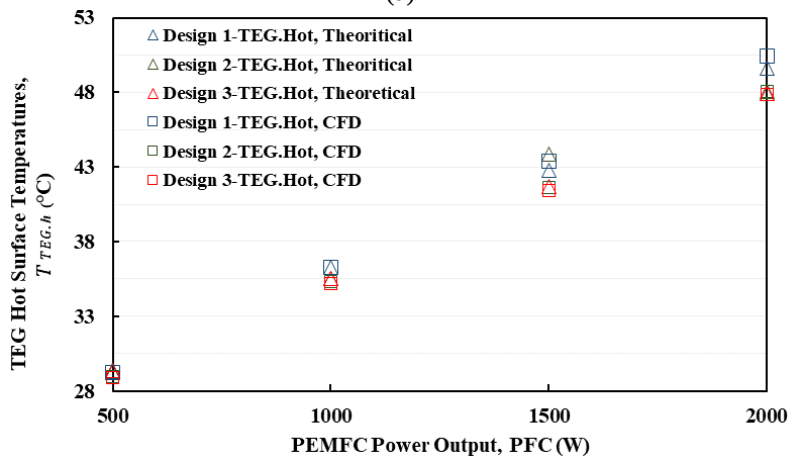

(b)

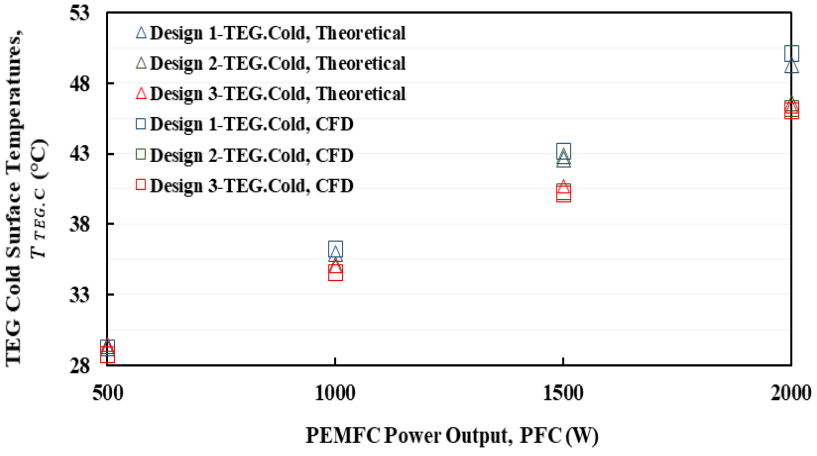

(c)

Fig. 7 - Temperature from simulations and theoretical on each IHR designs at 500-2000 W of PEMFC power (a) T_{H2}; (b) $T_{TEG.h}$; (c) $T_{TEG.C}$

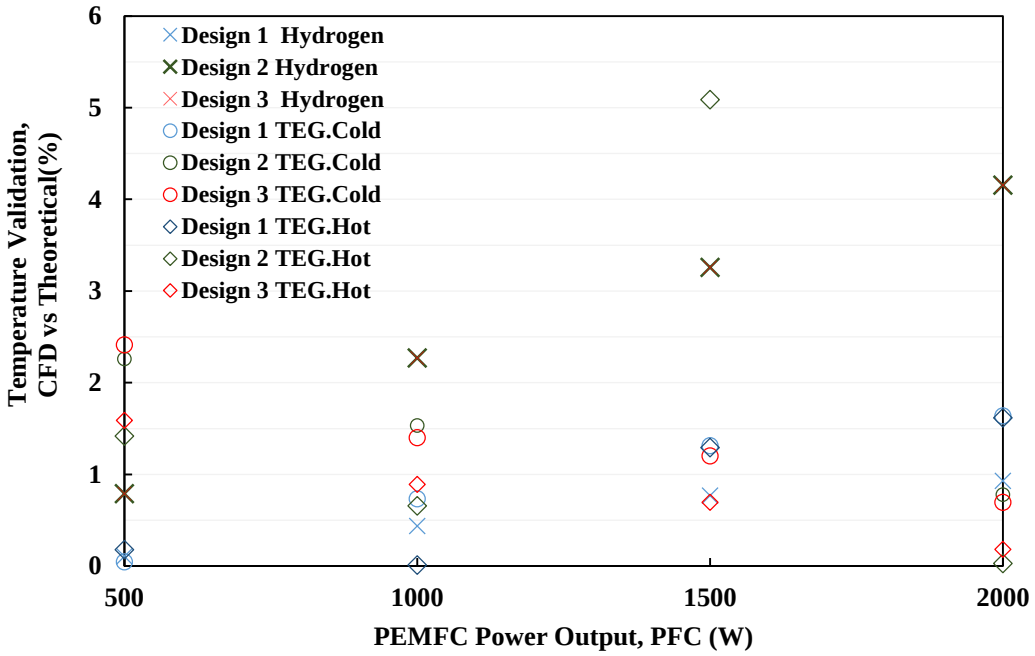

Fig. 8 - Temperature validation for T_{H2}, $T_{TEG.C}$, $T_{TEG.\ h}$ on each design with varied PEMFC power

3.2 Hydrogen Temperature Profile and Heating Degree

Fig. 9 shows the temperature profile of the hydrogen stream as it is heated by the waste heat from the PEM fuel cell at 1500 W and 2000 W electrical power outputs. Fig. 10a compares the hydrogen preheating degree that was achieved by all the IHR designs at different PEM fuel cell power outputs, while Fig. 10b provide the waste heat absorbed for the preheating purpose (using Eq. 3). Higher hydrogen preheating temperatures were achieved when the fuel cell power output increases due to the higher WHT from the stack. The targeted hydrogen exit temperature was 40 °C (a 10 °Cheating degree). The IHR designs were capable of reaching the targeted hydrogen temperature of 40ºC (or ΔT higher than 15 °C) only when the stack operates at 1500 W and 2000 W. At these fuel cell outputs, the hydrogen stream was successfully heated higher than its targeted temperature. At 1500 W fuel cell power, the hydrogen was preheated to 43 to 44ºC, while at 2000 W, the hydrogen preheating reaches 49 to 50ºC. The exit hydrogen temperatures for Design 1 is 5 to 6% higher than Designs 2 and 3 due to having 35% more heating surface area. The difference is small and negligible; therefore, Design 1 is not practical as it consumes more space and adds more weight to the vehicle power train system.

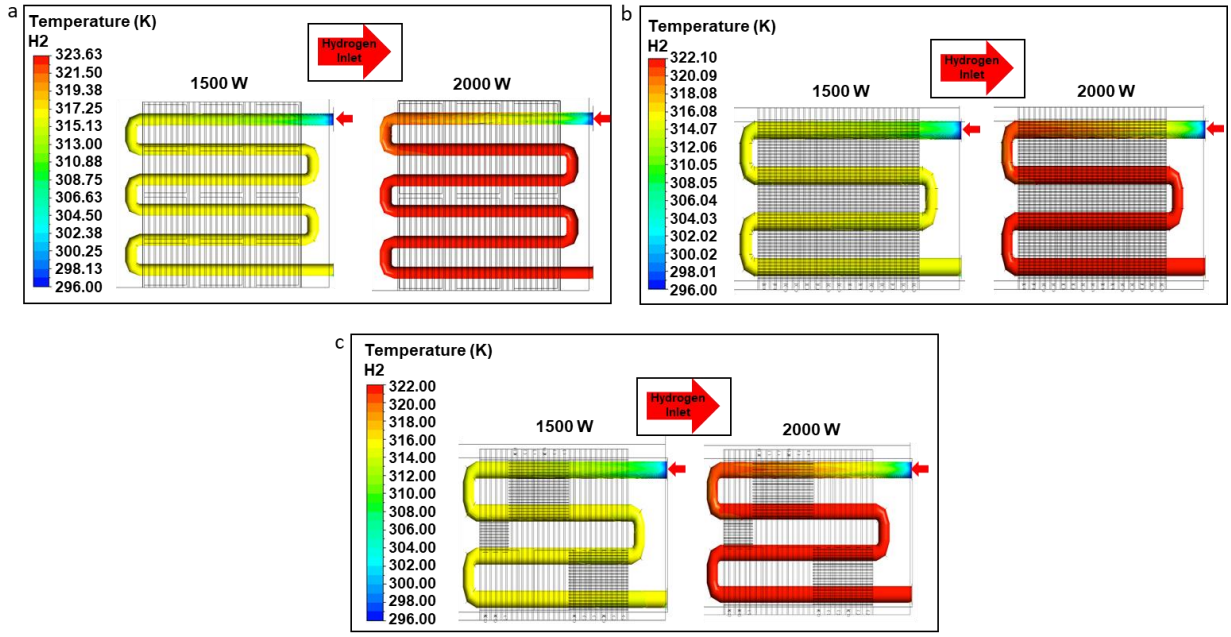

Fig. 9 - Hydrogen preheating temperature profiles for (1500, 2000) W on different designs; (a) Design 1; (b) Design 2; (c) Design 3

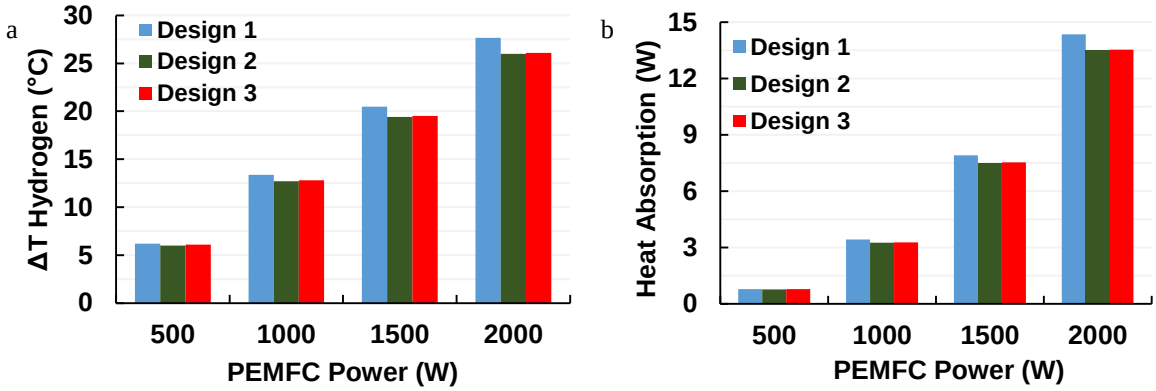

Fig. 10 - Heat exchanger designs on the PEMFC power generations against (a) Hydrogen temperature difference; (b) Heat absorption

To allow the IHR reach its hydrogen preheating target at lower fuel cell power, the fin and tube configurations must be revised. A higher fin surface area is needed to effectively allow heat transfer to the hydrogen stream when the waste heat stream temperature is low. The temperature profiles also indicate that the number of hydrogen tube-passes or length can be reduced as the heating reaches thermal saturation at half the length of the tube designs. This analysis shows that the IHR designs should have less tube-passes but higher fin surface areas, leading to designs with greater area-density.

Hypothetically, the introduction of elevated hydrogen temperatures into the PEM fuel cell stack will cause an effect to the water balance within the cells, either contributing to excessive flooding or severe membrane dehydration, It is a core issue in our continuous research in this area of study where the mass and energy balance of the fuel cell stack will be modelled to obtain the direct relationships between elevated hydrogen temperature, stack temperature, the power output and the water transport mechanism. It is expected that the modelling will provide information on the specific range of hydrogen temperature suitable for practice with minimal effect on water transport issues.

3.3 Theoretical Fuel Cell Power Enhancement due to Hydrogen Preheating

The PEM fuel cell power enhancement for each case and design is presented in Fig. 11. The power enhancement increases accordingly to the hydrogen temperatures exiting the preheating process. In general, the power gained by Design 1 is slightly higher than the other designs due to its higher hydrogen temperatures entering the stack. Overall, significant enhancements from the fuel cell nominal power output can be obtained as listed in Table 6. At 500 W of nominal power, the power enhancement is merely 1.7 to 2%, but the enhancement is 7.7 to 8% when the nominal power is 2000 W. This is translated to an extra 150 to 160 W of electrical power due to hydrogen preheating, which is significant enough to improve the fuel economy of the FCV by a similar margin.

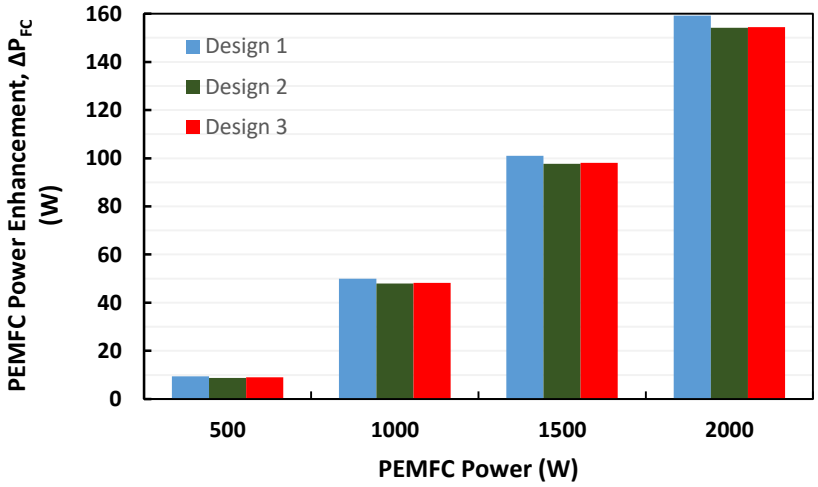

Fig. 11 - Power enhancement of PEMFC

Table 6 - Percentage of PEMFC power enhancement

Nominal Stack Output (W)	Stack Power Enhancement due to H2 Preheating (%)		
	Design 1	Design 2	Design 3
500	2.0	1.7	1.8
1000	5.0	4.8	4.8
1500	6.7	6.5	6.5
2000	8.0	7.7	7.7

3.4 TEG Temperature Profiles

Fig. 12 presents the temperature distribution on the TEG cells cold and hot surfaces at 2000 W of PEM fuel cell electrical power. The temperature profiles across the cells for Designs 1 and 2 are more uniform than Design 3 due to the configurations of the heat pipes. At the cold side, the cells nearest to the heat pipes have the lowest temperatures - TEG cells 4, 5 and 6 for Design 2 and TEG cells 3, 6, 9 and 12 for Design 1. The temperature difference between the surfaces fluctuate across the cells with a greater uniformity for Design 1 that produced the highest temperature difference of 0.72°C at cells 3, 6, 9 and 12. The highest temperature difference for Design 2 was at TEG cell 4 at 2.4°C and for Design 3 at TEG cell 2 at 2.3°C. Higher temperature difference for Designs 2 and 3 (approximately triple to Design 1) was caused by the use of a higher number of heat pipes that improved the cooling rate of the cells. These TEG temperature differences are comparable with those obtained by Sulaiman et al. [17] for a single cell experiment with a heat pipe directly fixed to the cell. however, Mohamed et al. [12] have shown that higher temperature difference can be achieved by enhancing the waste heat streamline using swirl generators. These results indicate that the optimal configuration for the cells-heat pipe-heat sink must be further explored to achieve greater temperature differences that lead to higher TEG power generation. Flow modifiers at the hot stream is also an option to improve convection heat transfer at the heating fins.

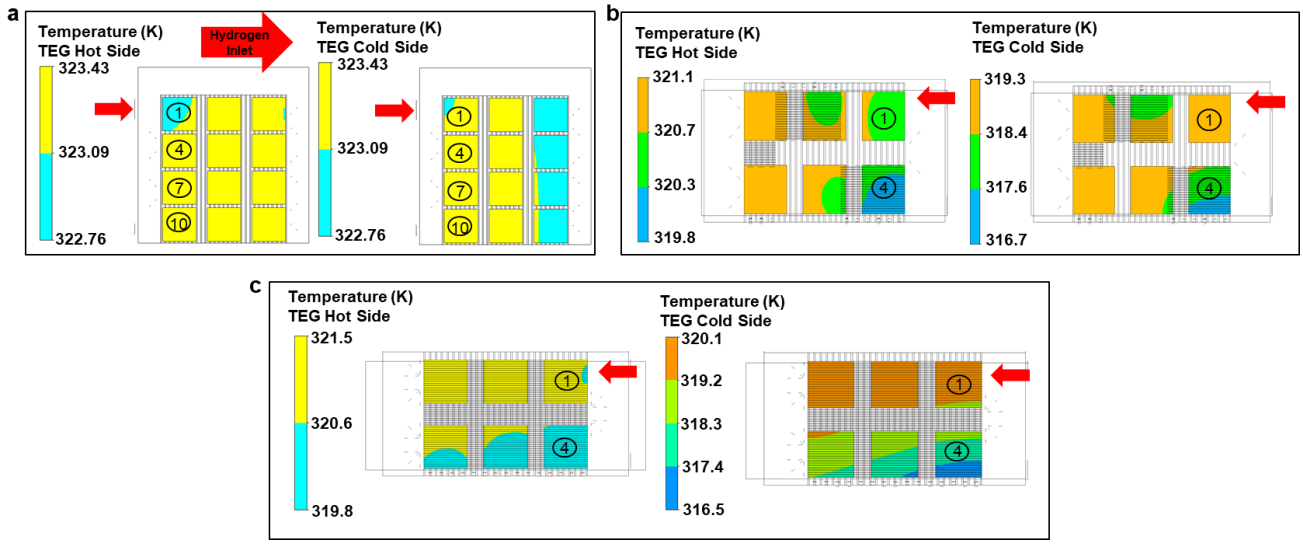

Fig. 12 - TEG surface temperatures at 2000W stack power (a) Design 1; (b) Design 2; (c) Design 3

3.5 TEG Power Output

The total power produced for the IHR designs increase exponentially to the WHT (relative to the PEM fuel cell power output). At 2000 W PEM fuel cell power, the maximum total TEG power produced from Design 1 is 550 μW, while for Designs 2 and 3 it is approximately 1400 μW. The amount of electrical power produced by the TEG cells is significantly lower compared to the electrical power enhancement due to hydrogen preheating. The amount is relatively lower from previous researches based on low grade waste heat. B. Singh et al. [20] reported a power between 3000 µW to 3400 µW with swirl nozzles while Sulaiman et al. [17] produced 230 μW at 60°C waste heat stream. The difference is due to the heterogeneous distribution of heat on the TEG hot-side as well as non-uniform cooling on the cold-side that caused fluctuating surface temperature differences and heat transfer rates across the cells. Designs 2 and 3 produced approximately 150% higher TEG power than Design 1 due to the use of almost doubled (7 more added heat pipes on design 2 and 3) more heat pipes in for cooling. The added heat pipes provided a better conduction heat transfer, releasing

more heat from the TEG modules to the cruised air streams, which enhanced the amount of electrical power generation. Future IHR design should consider installing more heat pipes to improve the cell cooling rate and uniformity. The system's available maximum WHT is 51 °C which is considered as an ultra-low grade waste heat with a 30°C cooling stream the tight temperature tolerance limits the TEG electrical power regeneration. The main heat transfer challenge for such conditions requires a very effective cooling and heating medium without compensating the compactness and light weight needed for an FCV. Despite the low power production from the TEG cells, it would still serve well as a secondary power regenerator for a FCV power train system as there is no extra cost in power consumption in the process. In the long run the continuous amount of accumulated recovered energy from the passive IHR system, would return the invested amount for the IHR system embedment on board an FCV.

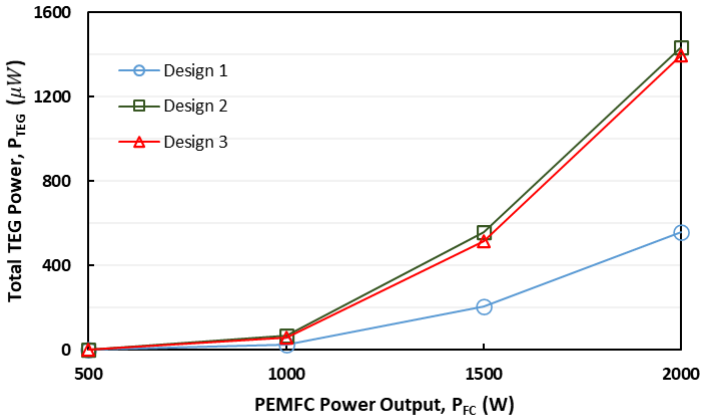

Fig. 13 - Total Power generated from TEGs

3.6 Waste Heat Utilization

Fig. 14 compares the percentage of recovered waste heat from the PEM fuel cell using Eqn. 4 that has included the regenerative effects for preheating the hydrogen fuel and TEG power generation. The waste heat utilization increases as higher WHT was released from PEM fuel cell to the IHR. Designs 2 and 3 are capable of effectively capturing the waste heat compared to Design 1, where the difference in waste heat utilization is in the range of 33 to 45%. The maximum waste heat utilization is only 1.6% at 2000 W of PEM fuel cell power. The main cause is due to the recovered heat from hydrogen preheating is limited to the controlled fuel feed rate based on the electrical power demand. In addition, the IHR has several layers of components that act as resistance to thermal flow, leading to a relatively low heat reaching the copper base plate and the TEG surface.

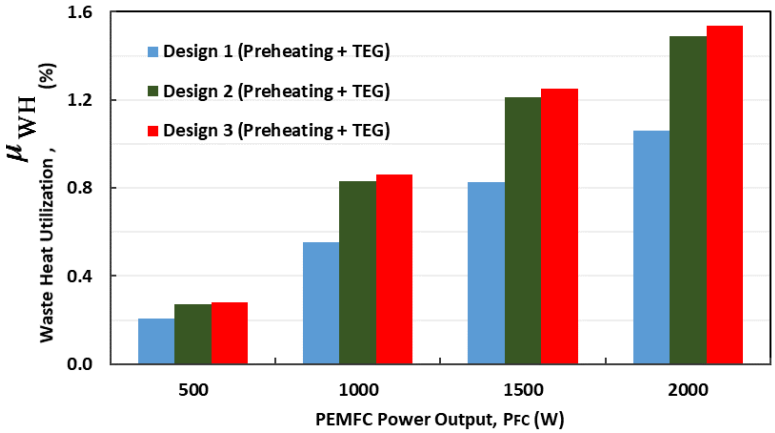

Fig. 14 - Heat exchanger designs waste heat utilization factors

3.7 Discussion

From previous work two separate PEM fuel cell WHR methods by TEG power generation [12] and hydrogen preheating [25] had improved the waste heat utilization and performance of an FCV. For IHR system, higher fuel cell operation increases hydrogen heating capabilities, which led to greater electrochemical reaction within the cells stack for power production. It also induces greater power production from TEG modules from the IHR system as higher thermal energy was produced from peak fuel cells operations. However, the main challenge for such low grade waste heat

recovery system on board an FCV is the space and weight constraints. It is crucial to maintain a bare minimal of additional weight and space while maintaining the demands for such IHR system. Thus, IHR system effectiveness are highly dependent the heating and cooling heat exchanger designs for an effective heat absorption and extraction. Other factors are the amount of available heat, which is linearly related to the stacks performances and the vehicle cruising speeds. As higher cruising speed provide greater convection of heat transfer [20].

For hydrogen preheating a multiple tube pass-fined heat exchanger concept provides a proficient heating domain [25]. Higher number of tube passes and longer fin length would increase the amount of heat absorbed but adds more weight and space. The additional surface areas generate extra heat transferred however, it is founded that heating heat exchangers from design 2 and 3 with four tube pass and shorter fins provided sufficient heating with the smallest overall system size that had achieved the targeted hydrogen heating temperatures. Future improvements would consider adaptation on previous corrugated tube design [26], where it was proven to achieve 8% fuel cell performance improvement with a single pass shell and tube concept. As an initial study of hydrogen preheating WHR method in current work focused on the percentage of improved performance by a simplified method discussed earlier. As highlighted from previous works fuel and stacks temperature elevations also interrupt the humidity levels on the fuel cells assembly which may leads to components degradation and greater diffusion resistance [4]. Another concern is the water content as higher reaction rates increases the water production which disturbs the water management of the stacks which opens flooding issues on the membrane assembly [3]. Thus, it is crucial for an in dept study on these consequences for a clear understanding on the behaviour of fuel cells towards elevated hydrogen fuel temperatures.

TEG devices in WHR systems provides additional power production which increases the fuel cell energy efficiency and waste heat utilization. The IHR cooling demands on TEG cold side was fulfilled with the heat pipe-heatsink heat exchanger design, this was also proved from other previous works [11, 12, 17, 18, 20]. The cooling heat exchanger designs 2 and 3 had proved that increasing the number of heat pipes generated better TEG power generation, due to the additional conduction heat transfer surface area is added from the added quantity of heat pipes. Other factors that affected TEG power generations are the heating heat exchangers, hot streams temperatures, speed and cooling air speed, temperatures. The multi-pass tube-finned heating heat exchanger design still could be further improved by inserting previous nozzle designs on a IHR system, as it is proven to absorb more heat. Table 7 displays a comparison with some WHR systems with TEG power generations that have been made by previous researchers.

Table 7 - Comparison of PEM fuel cell WHR from TEG power generations

References	**[12]**	**[20]**	**[11]**	**[17]**	**[18]**	**In this work**
Heat Recovery Method	Nozzle (heating) - Heat Pipe-Heatsink (cooling)	Swirl nozzle (heating) - Heat Pipe-Heatsink (cooling)	Heat Pipe-heatsink (cooling)	Heat Pipe-heatsink (cooling)	Heat Pipe (cooling)	Multi-Pass Finned-Tube (heating) - Heat Pipe-Heatsink (cooling)
Application	Parallel and series FCV power train WHR	FCV WHR	FCV WHR	FCV WHR	PEMFC WHR	FCV WHR
Heat Source	PEMFC operating from 1540 to 2150 W	PEMFC operating from 1200 to 2000 W	PEMFC operating at 2000 W	PEMFC operating at 1000 W	PEMFC operating at 900 W	PEMFC operating from 500 to 2000 W
Heat Source Temperature	40-60°C	45-60°C	53-58°C	24-37°C	24-37°C	29-51°C
Cooling Temperature	25°C	28°C	Ambient	23.5°C	23.5°C	30°C
Cooling fins	55	55	55	55	-	10-50
Cruising speed	100 km/h	0-36 km/h	0-36 km/h	20 km/h	4-8 km/h	36 km/h
Number of TEG cells	1 and 16	1	4	1	1	6 and 12

Methodology	Numerical	Experimental + Theoretical	Experimental	Experimental	Experimental	Numerical + Theoretical
Waste Heat utilization	2% with 16 TEG cells	-	-	-	-	< 1.6%
Power generated from TEG	3400 μW	3000 μW at 1.6 swirl number	1900 μW	218 mW	110 mW	1400 μW

4.0 Conclusions

A new IHR design concept for FCV WHR was introduced where the IHR combined hydrogen preheating process to increase the PEM fuel cell power output with direct electrical power generation using TEG cells. Three IHR designs were evaluated in this initial study using computational numerical analysis and validated with theoretical heat exchanger and TEG models. For this evaluation, the cooling of the TEG cells through the heat pipe-heat sink system was fixed relative to the assumption that the FCV was cruising at its design of 36 kmh-1 at an ambient temperature of 30°C. Under these conditions the findings are concluded as follows:

(i) The IHR system simulations is able to predict the preheated hydrogen temperature and TEG surface temperatures with a maximum percentage different of 5% in validation with the theoretical model. Additional to that the designs also had achieved the targeted 40°C hydrogen preheating temperature.

(ii) The adapted passive heat exchanger designs of multi-pass tube finned combined with heat pipe-heatsink in the IHR system, succeeded to secure the heating and cooling demands for simultaneous fuel preheating and TEG power production. Which would lead to progressive FCV fuel saving.

(iii) The Hydrogen stream temperature and the TEG surface temperatures simulated are dependent on the power output of the Horizon H2000 stack. The response is in an increasing linear relation, this is due to the greater available amount of waste heat produced from the stack on higher output operations.

(iv) The proposed designs are only suitable when the fuel cell power is 1500 W to 2000 W with a maximum fuel cell power increment of 8% due to hydrogen preheating and production of 1400 μW from TEG modules. This significant enhancement would lead to greater fuel economy for the FCV and allow hydrogen fuel cells to be economically attractive for the transportation sector.

(v) The power output of the TEG cells is comparatively small to the enhanced power outputs of the fuel cell stack due to hydrogen preheating. Significant outputs between 500 to 1400 μW were obtained only when the fuel cell power output was 1500 W to 2000 W due to waste heat stream higher temperatures.

(vi) Design 3 best fits for an FCV WHR system as it provided the smallest overall system size with a greater secondary power production at a cost of insignificant fuel preheating performance reduction.

(vii) Further explorations on geometries and systems design are needed to achieve greater area density for the heating heat exchanger and cooling heat sinks are required before the IHR concept can be considered feasible. At this stage, the regeneration of waste heat energy is still under utilize which is below 1.6%.

(viii) Future works should increase the quantity of heat pipes used at the cooling heat exchanger for a greater TEG surface heat extraction and power generations. Another recommendation on improving the TEG power output is additional quantity of TEG.

Acknowledgement

The authors would like to thank Universiti Teknologi MARA (UiTM) for the facilities and Ministry of Education Malaysia for the financial support given under 600-RMC/KKP 5/3 (002/2021).

REFERENCES

[1] L Ren, S Zhou, X Ou, Life-cycle energy consumption and greenhouse-gas emissions of hydrogen supply chains for fuel-cell vehicles in China, Energy 209, 2020, 118482.

[2] G Wang, Y Yu, H Liu, C Gong, S Wen, X Wang, Z Tu, Progress on design and development of polymer electrolyte membrane fuel cell systems for vehicle applications: A review, Fuel Processing Technology 179, 2018, 203-228.

[3] Raja Arif, R. M. A. Effects of high-temperature operating conditions on the through-plane gas permeability of gas diffusion layers used in PEFCs. Journal of Applied Engineering Design and Simulation, 1(1), (2021), 1-11. https://doi.org/10.24191/jaeds.v1i1.3.

[4] Baroutaji A et al., Advancements and prospects of thermal management and waste heat recovery of PEMFC, Int J Thermofluid 9 (2021), 100064.
[5] IA Zakaria, WANW Mohamed, AMI Mamat, MR Mustaffa, Steady-state potential energy recovery modeling of an open cathode PEM fuel cell vehicle, Applied Mechanics and Materials Vols. 465-466 (2014) pp 114-119. doi:10.4028/www.scientific.net/AMM.465-466.114.
[6] IA Zakaria, WANW Mohamed, MB Zailan, WH Azmi, Experimental analysis of SiO2-Distilled water nanofluids in a Polymer Electrolyte Membrane fuel cell parallel channel cooling plate, Int. J of Hydrogen Energy 44 (2019): 25850-25862.
[7] WANW Mohamed, SFA Talib, IA Zakaria, AMI Mamat, WRW Daud, Effect of Dynamic Load on the Temperature Profiles and Cooling Response Time of a Proton Exchange Membrane Fuel Cell, Journal of the Energy Institute 91(3) (2018) 349-357.
[8] He T, Shi R, Peng J, Zhuge W, Zhang Y. Waste heat recovery of a PEMFC system by using Organic Rankine Cycle. Energies 9 (2016), 267. http://dx.doi.org/10.3390/en9040267.
[9] Hwang JJ, et al., Implementation of a heat recovery unit in a proton exchange membrane fuel cell system, Int. J. Hydrogen Energy 35(16) (2010), 8644-53.
[10] S. Khanmohammadi, M. Rahmani, F. Musharavati, S. Khanmohammadi, and Q.-V. Bach, Thermal modeling and triple objective optimization of a new compressed air energy storage system integrated with Rankine cycle, PEM fuel cell, and thermoelectric unit, Sustain. Energy Technol. Assessments, vol. 43, p. 100810, 2021, doi: 10.1016/j.seta.2020.100810.
[11] Hamdan, M. H. ., Mat Som, N. A., Amirul Abdul Rashid, & Gilbert Jugi Jimmy. (2021). Performance analysis on series and parallel circuit configurations of a four-cell thermoelectric generator module design. Journal of Applied Engineering Design and Simulation, 1(1), 32-42. https://doi.org/10.24191/jaeds.v1i1.18.
[12] WANW Mohamed, B Singh, MF Mohamed, AM Aizuwan, ABM Zubair, Effects of fuel cell vehicle waste heat temperatures and cruising speeds on the outputs of a thermoelectric generator energy recovery module, Int. J of Hydrogen Energy 46 (2021), 25634-25649.
[13] Remeli MF, Tan L, Date A, Singh B, Akbarzadeh A. Simultaneous power generation and heat recovery using a heat pipe assisted thermoelectric generator system. Energy Convers. Manag. 2015; 91: 110-19.
[14] Goldsmid H. Bismuth telluride and its alloys as materials for thermoelectric generation. Materials 2014; 7: 2577–92.
[15] Luo D, Wang R, Yu W, Sun Z, Meng X, Theoretical analysis of energy recovery potential for different types of conventional vehicles with a thermoelectric generator. Energy Procedia 2019; 158: 142–47.
[16] Gao X, Andreasen SJ, Chen M, Kaer SK, Numerical model of a thermoelectric generator with compact plate-fin heat exchanger for high temperature PEM fuel cell exhaust heat recovery. Int. J. Hydrogen Energy 2012; 37 (10): 8490–98.
[17] Sulaiman MS, Singh B, Mohamed WANW. Experimental and theoretical study of thermoelectric generator waste heat recovery model for an ultra-low temperature PEM fuel cell powered vehicle. Energy 2019; 179: 628-46.
[18] Sulaiman MS, Mohamed WANW, Singh B, Ghazali MF. Validation of a waste heat recovery model for a 1 kW PEM fuel cell using thermoelectric generator. 2017 IOP Conf. Ser.: Mater. Sci. Eng. 226 (1) 012148.
[19] Guo X, et al., Energetic and exergetic analyses of a combined system consisting of a high-temperature polymer electrolyte membrane fuel cell and a thermoelectric generator with Thomson effect, Int. J. Hydrogen Energy 2019; 44(31): 16918-32.
[20] B. Singh, W. A. N. W. Mohamed, M. N. F. Hamani, and K. Z. N. A. So, "Enhancement of low grade waste heat recovery from a fuel cell using a thermoelectric generator module with swirl flows," Energy vol. 236, 2021, doi: 10.1016/j.energy.2021.121521.
[21] Gao X, Andreasen SJ, Kaer SK, Rosendahl LA, Optimization of a thermoelectric generator subsystem for high temperature PEM fuel cell exhaust heat recovery. Int. J. Hydrogen Energy 2014; 39 (12): 6637–45.
[22] Gao X, Andreasen SJ, Chen M, Kaer SK, Potential usage of thermoelectric devices in a high temperature polymer electrolyte membrane (PEM) fuel cell system: Two case studies. J. Electron. Mater. 2012; 41 (6): 1838–44.
[23] Högblom O and Andersson R, Multiphysics CFD simulation for design and analysis of thermoelectric power generation. Energies 2020; 13: 4344; doi:10.3390/en13174344.
[24] Chen W-H, Lin Y-X, Chiou Y-B, Lin Y-L, Wang X-D, A computational fluid dynamics (CFD) approach of thermoelectric generator. Appl. Therm. Eng. 2020; 173: 115203.
[25] WANW Mohamed and MHM Kamil, Hydrogen preheating through waste heat recovery of an open-cathode PEM fuel cell leading to power output, Energy Conversion and Management 09/2016; 124:543-555.
[26] Q. Zhang, Z. Tong, S. Tong, and Z. Cheng, "Research on low-temperature heat exchange performance of hydrogen preheating system for PEMFC engine," Int. J. Hydrogen Energy, vol. 45, no. 55, pp. 30966–30979, 2020, doi: 10.1016/j.ijhydene.2020.08.076.
[27] H. Q. Nguyen, A. M. Aris, and B. Shabani, "PEM fuel cell heat recovery for preheating inlet air in standalone solar-hydrogen systems for telecommunication applications: An exergy analysis," Int. J. Hydrogen Energy, vol. 41, no. 4, pp. 2987–3003, 2016, doi: 10.1016/j.ijhydene.2015.12.108.

[28] T. Choi and T. Y. Kim, "Three-zone numerical modeling method for predicting system-level waste heat recovery performance of thermoelectric generator with various electrical array configurations," Energy Convers. Manag., vol. 240, p. 114270, 2021, doi: 10.1016/j.enconman.2021.114270.
[29] W. H. Chen, Y. X. Lin, Y. Bin Chiou, Y. L. Lin, and X. D. Wang, "A computational fluid dynamics (CFD) approach of thermoelectric generator (TEG) for power generation," Appl. Therm. Eng., vol. 173, Jun. 2020, doi: 10.1016/J.APPLTHERMALENG.2020.115203.
[30] YA Cengel and AJ Ghajar, Heat and Mass Transfer, Fifth Edition, 2015, McGraw Hill, New York.
[31] S. Vijayaraghavan, R. Shah, and D. V. Kumar, "Materials Today : Proceedings A comparison study on thermal performance enhancement of corrugated oil cooler with internal turbulators – Numerical and experimental approach," Mater. Today Proc., no. xxxx, 2022, doi: 10.1016/j.matpr.2021.10.052.
[32] Z. Zhong, L. Meng, X. Li, G. Zhang, Y. Xu, and J. Deng, "Enhanced heat transfer performance of optimized micro-channel heat sink via forced convection in cooling metal foam attached on copper plate," J. Energy Storage, vol. 30, no. April, p. 101501, 2020, doi: 10.1016/j.est.2020.101501.
[33] R. Yakut, K. Yakut, F. Yeşildal, and A. Karabey, "Experimental and Numerical Investigations of Impingement Air Jet for a Heat Sink," Procedia Eng., vol. 157, pp. 3–12, 2016, doi: 10.1016/j.proeng.2016.08.331.
[34] N. F. Jamaludin, F. Mohamed Yusop, and N. Saji, "Study Usage of Computational Fluid Dynamics (CFD) For Indoor Simulation", peat, vol. 2, no. 1, pp. 453-463, Jun. 2021.